Research article

Improved Otsu and Kapur approach for white blood cells segmentation based on LebTLBO optimization for the detection of Leukemia

Nilkanth Mukund Deshpande[1,2], Shilpa Gite[3,4,*], Biswajeet Pradhan[5,6], Ketan Kotecha[3,4] and Abdullah Alamri[7]

[1] Department of Electronics and Telecommunication, Lavale, Symbiosis Institute of Technology, Symbiosis International (Deemed University), Pune 412115, Maharashtra, India
[2] Electronics and Telecommunication, Vilad Ghat, Dr. Vithalrao Vikhe Patil College of Engineering, Ahmednagar 414111, India
[3] Department of Computer Science, Lavale, Symbiosis Institute of Technology, Symbiosis International (Deemed University), Pune 412115, Maharashtra, India
[4] Symbiosis Center for Applied Artificial Intelligence, Lavale, Symbiosis International (Deemed University), Pune 412115, Maharashtra, India
[5] Centre for Advanced Modelling and Geospatial Information Systems, School of Civil and Environmental Engineering, Faculty of Engineering and IT, University of Technology Sydney, NSW 2007, Sydney, Australia
[6] Earth Observation Centre, Institute of Climate Change, Universiti Kebangsaan Malaysia, 43600 UKM, Bangi, Malaysia
[7] Department of Geology and Geophysics, College of Science, King Saud University, Riyadh 11451, Saudi Arabia

* **Correspondence:** Email: shilpa.gite@sitpune.edu.in.

Abstract: The diagnosis of leukemia involves the detection of the abnormal characteristics of blood cells by a trained pathologist. Currently, this is done manually by observing the morphological characteristics of white blood cells in the microscopic images. Though there are some equipment-based and chemical-based tests available, the use and adaptation of the automated computer vision-based system is still an issue. There are certain software frameworks available in the literature; however, they are still not being adopted commercially. So there is a need for an automated and software- based framework for the detection of leukemia. In software-based detection, segmentation is the first critical stage that outputs the region of interest for further accurate diagnosis. Therefore,

this paper explores an efficient and hybrid segmentation that proposes a more efficient and effective system for leukemia diagnosis. A very popular publicly available database, the acute lymphoblastic leukemia image database (ALL-IDB), is used in this research. First, the images are pre-processed and segmentation is done using Multilevel thresholding with Otsu and Kapur methods. To further optimize the segmentation performance, the Learning enthusiasm-based teaching-learning-based optimization (LebTLBO) algorithm is employed. Different metrics are used for measuring the system performance. A comparative analysis of the proposed methodology is done with existing benchmarks methods. The proposed approach has proven to be better than earlier techniques with measuring parameters of PSNR and Similarity index. The result shows a significant improvement in the performance measures with optimizing threshold algorithms and the LebTLBO technique.

1. Introduction

Leukemia is always considered being a life-scaring disease [1]. It attacks the blood-forming capacity of bone marrow [2−4]. Bone marrow generates leukocytes (white blood cells) gradually through different stages involving the generation of the blast cells [5]. Due to the development of leukemia, these blasts cells in the human blood tend to increase [6]. A higher amount of blasts cells and other abnormal cells lead to severe leukemia [7]. The detection is the task of observing the morphologies of leukocytes and predicting the type and severity of leukemia [8].
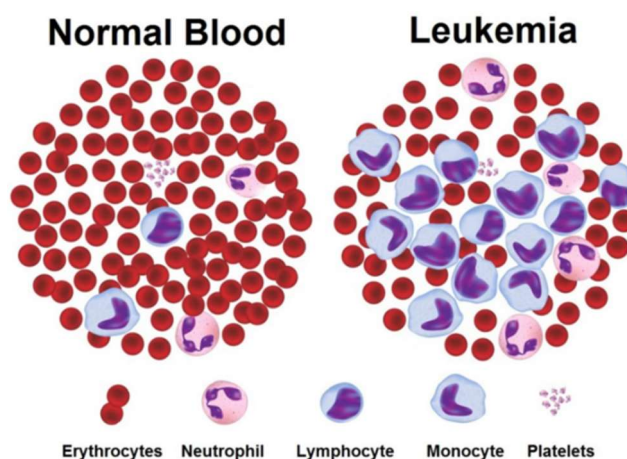

Figure 1. Normal and leukemia cells [9].

It has four broad types: acute myeloid leukemia (AML), acute lymphoblastic leukemia (ALL), chronic myeloid leukemia (CML) and chronic lymphoblastic leukemia (CLL) [10]. In addition, there is the existence of the components like blasts cells (immature leukocytes), Auer rods (a very thin rod like structure) in the blood sample of leukemia patients.

Figure 1 shows the microscopic image of the blood cells having normal and leukemia cells [9]. Microscopic analysis is required to detect the presence of leukemia cells [11]. Figure 1 indicates that leukemia cells differ morphologically from normal cells. The diagnosis of leukemia involves the

detection of these abnormal characteristics of blood cells [12]. The very first and the important step in the detection is segmentation [13]. In the microscopic image of a stained blood sample, there are many components, including leukocytes-white blood cells, erythrocytes-red blood cells, plasma, and parasites [14]. Staining is required for making the blood smear for microscopic analysis [15,16]. Segmentation in leukemia detection involves separating leukocytes from the given stained blood microscopic image to get the region of interest [17]. The popular segmentation techniques are thresholding [18], clustering [19], edge-based segmentation [20], region-based segmentation [21], artificial neural network-based segmentation [22], and partial differential equation-based segmentation [23]. However, a generalized segmentation methodology involves pre-processing, background separation, and the outcome will be the region of interest for further detection purposes [24].

In the proposed methodology, Otsu and Kapur thresholding are utilized for the segmentation of leukocytes. Furthermore, to enhance the thresholding performance, computational time utilization, and optimization, the learning enthusiasm-based teaching-learning-based optimization (LebTLBO) is used. It has been successfully used in various science and engineering applications in recent years. In the traditional teaching-learning-based optimization (TLBO)and most of its variants, all learners have an equal chance of learning from others. LebTLBO was inspired by the learner's varied chances of acquiring knowledge compared to others, and it incorporated a learning excitement mechanism into the basic TLBO [25].

This optimization involves the teaching-learning process in the class [26]. In this algorithm, there are three phases of working, namely teaching phase, learning phase, and poor student tutoring phase [27]. Broadly, in this case, the students with a good desire to take knowledge from their teacher will get good grades and alter their positions towards top. Students with less desire will fall to the bottom, and will not update their positions towards the top. In addition to this, the poor phase is also present, which analyzes the same thing for poor students. Here poor students are those who falls within the lower 10% of the whole class. The learning desire of the poor students is also analyzed and their positions are also considered to be updated. So this involves the position alteration of good students as well as poor students, giving more precise optimization [28]. The same is explained in more depth in Section 3.

The paper is divided into six different sections. Section 1 presents the introduction. Section 2 talks about the related work. Section 3 explores the proposed technique for segmentation with a detailed methodology. Different performance metrics are explained in Section 4. Finally, Section 5 contains the results and discussion, followed by the conclusion and future scope.

2. Related work

There are different segmentation methods employed for the white blood cell separation for the detection of leukemia by different researchers including mathematical morphology, fuzzy logic approach [29], watershed transform [30], k-means clustering [31], zack algorithm [32], marker controlled watershed transform [33], clustering based on stimulating discriminant measures (SDM) [34,35], hough transform [36], iterative thresholding with watershed transform [37], edge thresholding, triangular thresholding DOST algorithm [38], Otsu's method [39,40], a conventional neural network with laplacian of gaussian (LOG) and coupled edge profile active contours (C-EPAC) [41], sequential maximum angle convex cone (SMACC) clustering with iterative) algorithm and iterative self-organizing data analysis technique algorithm (ISODATA), and local binary pattern (LBP) [39], VGG16 segmentation [42].

The methods adopted by researchers are mainly Otsu thresholding which becomes a time-consuming technique when the number of threshold levels are increased [43] and needs an appropriate tuning for proper threshold selections [44,45]. The majority of methods adopting the thresholding concept [46−48] employed the binary classification of images, where the image is divided into background and foreground only. But the blood microscopic images comprise of 4 to 5 different parts. These include leukocyte, erythrocytes, platelets, plasma parasites (due to the cause of some infections). The development of leukemia in the human body, causes the generation of immature leukocytes (blasts cells), and other morphological component such as Auer rod in the blood. Therefore, the investigation comprises of the separation of these 4 to 5 components and detection of the morphological abnormalities in the blood cell images. Hence, it is very challenging to adopt binary thresholding methods for segmentation purposes.

Figure 2 shows the different parts in the microscopic image of blood-leukocyte, erythrocyte [49]. The blood image can contain plasma and some parasites as well. So, it is very difficult to segment the image with binary thresholding. As a result, more than one threshold is required for segmentation to separate these various components. Therefore, there is a need to adopt a multi-level thresholding technique for blood microscopic images. Artificial intelligence and deep learning-based methods will take a significant time for performing the segmentation due to the requirement of more iterations for better results. Most times, where deep learning may be adopted, there is a need to use tuned hyper-parameters to carry out the segmentation. These tuning always influences the performance of the model [50].
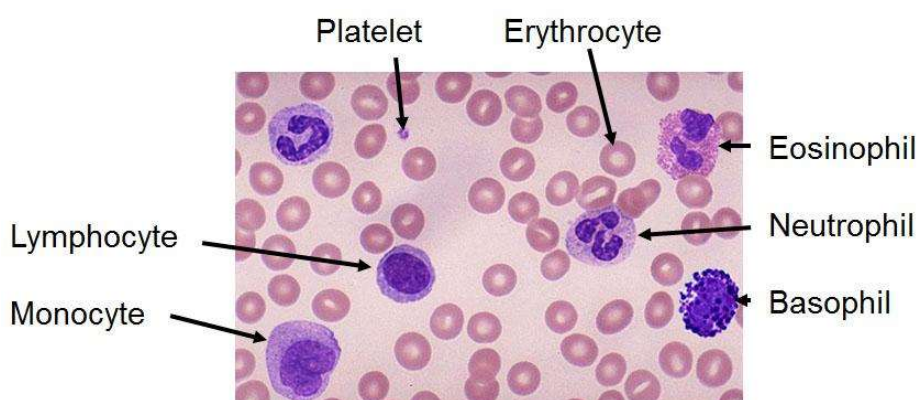

Figure 2. Different parts of microscopic blood image [51].

It also deals with the problems of under-fitting and over-fitting. So proper tuning of hypermeters is always an important issue in deep learning models. This tuning process is time-consuming and is also a resource-consuming task [52,53]. One more problem with deep learning algorithms is the requirement of very large datasets for better results [54,55]. As leukemia is cancer and its infected patients are comparatively in fewer numbers, it is difficult to get a large number of imaging samples for building a larger dataset. On the other hand, traditional image processing algorithms perform well with a small number of dataset images. Clustering is one more approach for segmentation that requires the user to initialize the cluster priory, which is the drawback of the same [56].

There are also different issues during image capturing, such as resolution, the contrast which are

to be considered when these methods are to be used for segmentation purposes [57]. Otsu is the most popular thresholding method of segmentation [58]. Time expensiveness is the major drawback of this algorithm; it has very high time consumption [59]. According to Tuba [44] for 10 threshold levels, this algorithm requires a time of about 10,000 years with an I-7processor [44].

Therefore, the aforementioned issues have motivated the authors to come up with different optimization techniques to be adopted for image segmentation purposes. Figure 3 shows the different optimization techniques.

All evolutionary and swarm intelligence-based algorithms are probabilistic, and they all require the same set of regulating parameters, such as population size, generation number, elite size, and so on. Different algorithms require their algorithm-specific control parameters, in addition to the common control parameters as explained in Table 1.

Table 1. Algorithm specific control parameters.

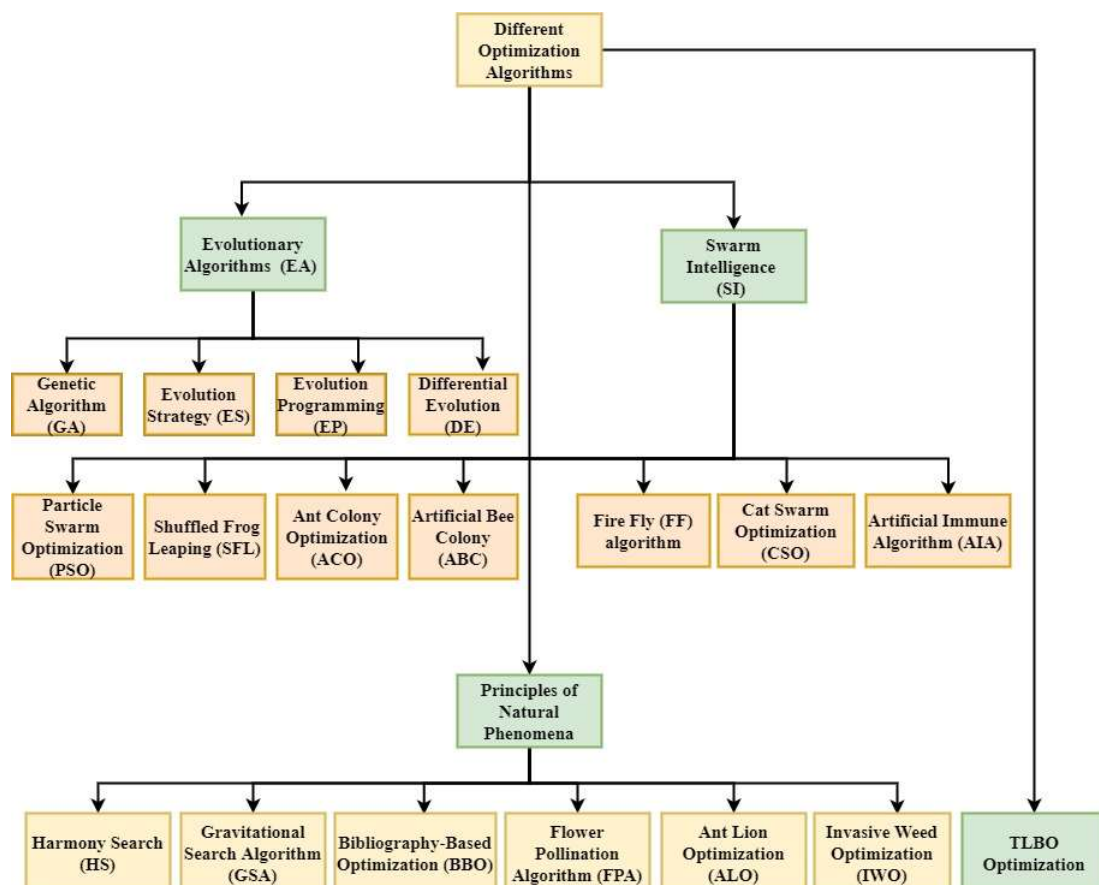| Algorithm	Control parameters
GA	Mutation probability, crossover probability and the selection operator.
ABC	Number of spectator bees, employed bees, scout bees and limit.
PSO	Inertia weight, social and cognitive parameters.
Harmony search	Memory consideration rate, pitch adjustment rate and the number of improvisations are all factors in the HS algorithm.

Figure 3. Different optimization algorithms used in the literature.

Algorithm-specific parameters are generally modified when using optimization algorithms [60]. The correct tuning of algorithm-specific parameters is a critical aspect that influences the performance of the algorithms discussed above. Incorrect tuning of algorithm-specific parameters either increases processing effort or produces the local best solution. Rao et al. [61] recognized this and developed the TLBO algorithm, which does not require any algorithm-specific parameters [62]. For the TLBO algorithm to work, it only needs a few basic governing parameters, like population size and generation number. Among optimization researchers, the TLBO algorithm has acquired widespread popularity [63].

From the discussion of the above methods, there is a need for a simple and less time-consuming technique for segmentation. Though there are a variety of optimization algorithms, the TLBO and its variant learning enthusiastic type prove to be simple and time inexpensive, as explained in the previous paragraph. For that reason, LebTLBO is adopted in this work.

3. The proposed segmentation approach

Input microscopic images of the stained blood sample are taken from publicly available databases[1]. The segmentation methodology can be explained as below. Table 2 shows the dataset images of ALL-IDB dataset.

Table 2. ALL-IDB dataset description.

Name	Image formats	Number of images	Color depth	Remark
ALL-IDB-1	JPEG	109 (510 lymphoblast)	24-bit, 2592 × 1944	Cancerous
ALL-IDB-2	JPEG	260 (130 lymphoblast)	24-bit 257 × 257	Cancerous

1) Images loading: The images are taken from the publicly available databases. It consists of the microscopic images of stained blood smears of normal and leukemia infected patients. Here, ALL-IDB dataset is considered for the study and implementation of the algorithm [64−66]. This database has two parts ALL-IDB-1 consisting of 260 images of normal and leukemia patients, and ALL-IDB2 has 106 images of normal and leukemia patients.

2) Pre-processing: The images obtained from the microscope may have certain errors during the image capturing. Also, there is a requirement for images to convert in grayscale format for further processing. So the database images are gray-scaled for further processing.

3) Segmentation: The images are parsed in the further stage of segmentation. It involves the extraction of the region of interest. For detection of leukemia, white blood cell-leukocytes are the region of interest in the blood smear microscopic images, which are to be the outcome of segmentation. A broader classification of segmentation methods includes thresholding, edge-based methods, region-based methods, clustering methods, watershed-based methods, artificial neural network-based methods, etc. [67].

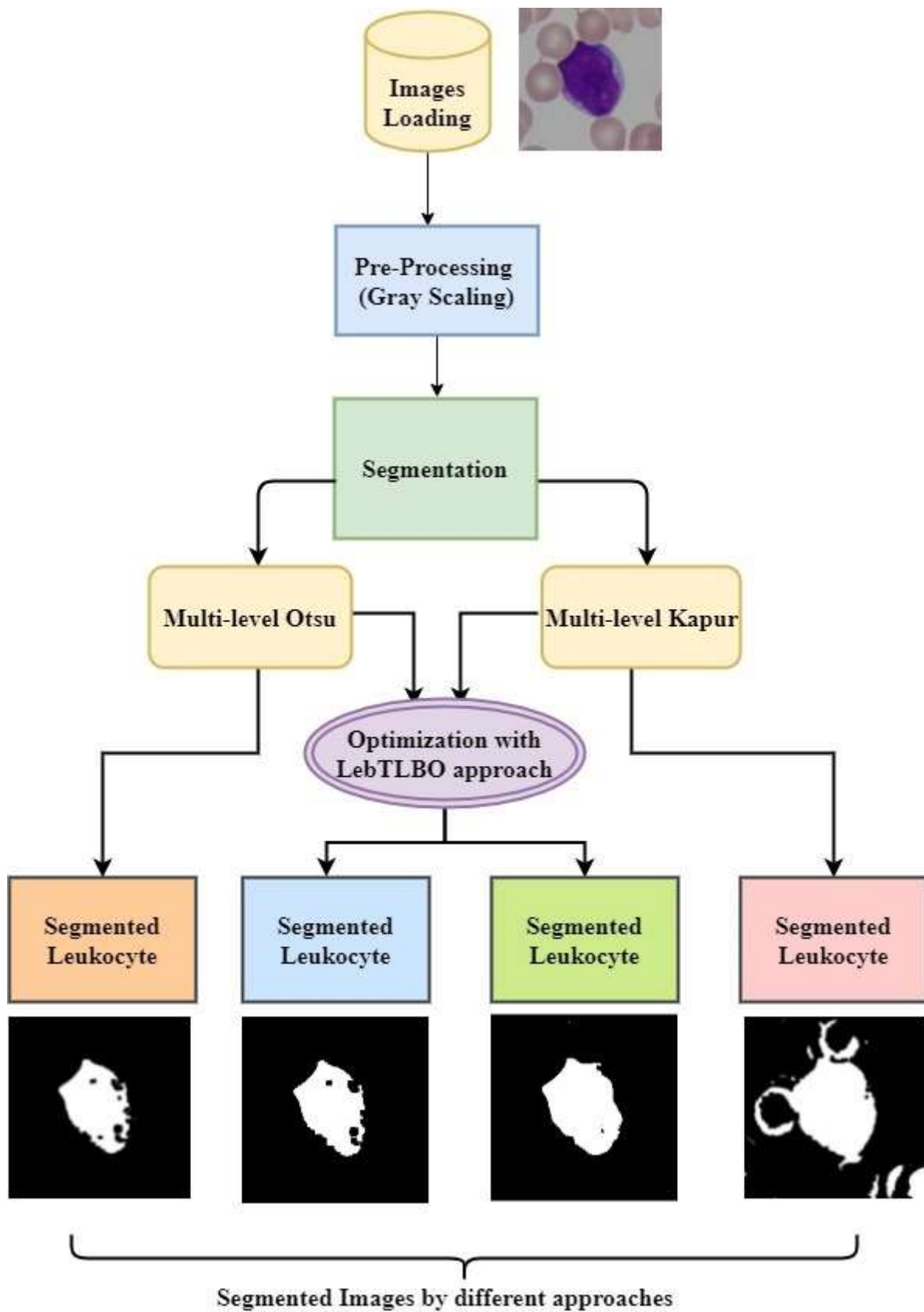[1] (Available at https://homes.di.unimi.it/scotti/all/)

Figure 4. Proposed approach for segmentation.

Figure 4 shows the proposed approach for segmentation for leukemia detection purposes.

Out of the different segmentation methods stated earlier in Section 2, thresholding is the most simple and easy step towards segmentation for separating foreground and background in an image. It is further sub-divided into local and global thresholding [68]. Global thresholding uses an image as a whole, while distinguished characteristics of local image areas may be used to choose thresholds of the image in local thresholding type. The methods adopted here are Otsu and Kapur multi-level thresholding for the problem formulation, optimizing each of them using LebTLBO [26]. Following are the different concepts used for segmentation.

3.1. Multilevel thresholding

The most important concept utilized here is multi-level thresholding rather than binary thresholding because binary threshold divides the image into two major parts-background and foreground. In the case of blood microscopic images, there are different components, including plasma, leukocyte, erythrocytes, and some other cells like parasites. So for segmentation, there is a need for more than one threshold to separate these different components. Hence, multi-level thresholding is preferred over binary type. In multi-level thresholding, more than two thresholds are generally used.

So instead of generating only two regions, as in the case of bi-level thresholding, multi-level thresholding generates several regions such as $[r_1, r_2, r_3, r_4, \ldots \ldots r_n]$ cconsidering the thresholding values, and this can lead to more accurate results of segmentation. In addition, different threshold values, such as $th_1, th_2, th_3, th_4 \ldots \ldots$ tc are considered in this case. Equation 1 could further explore this.

$$
\begin{aligned}
&r_1 \leftarrow d(m,n), \text{if } 0 < d(m,n) < th_1 \\
&r_2 \leftarrow d(m,n), \text{ if } th_1 < d(m,n) < th_2 \\
&r_3 \leftarrow d(m,n), \text{ if } th_2 < d(m,n) < th_3 \\
&r_i \leftarrow d(m,n), \text{ if } th_i < d(m,n) < th_{i+1} \\
&\ldots r_k \leftarrow d(m,n), \text{if } Th_{ne-1} < d(m,n) < Th_{ne}
\end{aligned}
\tag{1}
$$

where ne are the number of threshold levels.

3.2. Otsu method

For multi-level thresholding in the segmentation, Otsu and Kapur-based algorithms are the most popular [69]. Otsu comes under the global method of image thresholding [70]. Amongst the different thresholding methods, multi-level Otsu is more popular among the researchers [71,72]. Otsu maximizes the variances between the classes. The strategy here is to process the image histogram and segment the objects by minimizing the thresholds into the different classes. Generally, image histograms may contain two clear peaks representing different intensity ranges. The intra-class variance, defined as the weighted sum of the variances between the two classes, is minimized by finding a threshold, as shown in Eq (2).

$$
\sigma_\omega^2(t) = \omega_0(t)\sigma_0^2(t) + \omega_1(t)\sigma_1^2(t)
\tag{2}
$$

Weights ω0 and ω1 are probabilities of different classes, t defines the threshold value, and σ_0 and σ_1 are the class variances. The histogram is used to obtain the class probability, $\omega_{0,1}$ (t) is calculated

from L bits of the histogram.

$$\omega_0(t) = \sum_{i=0}^{t-1} p(i) \tag{3}$$

$$\omega_1(t) = \sum_{i=t}^{L-1} p(i) \tag{4}$$

For two classes, minimization of the intra-class variance is the same as maximizing the inter-class variance.

$$\sigma_b^2(t) = \sigma^2 - \sigma_\omega^2(t) \tag{5}$$

$$= \omega_0(t)\omega_1(t)[\mu_0(t) - \mu_1(t)]^2$$

The class means $\mu 0(t)$, $\mu 1(t)$ and μT are given by

$$\mu_0(t) = \frac{\sum_{t=0}^{t-1} p(i)}{\omega_0(t)} \tag{6}$$

$$\mu_1(t) = \frac{\sum_{i=t}^{L-1} p(i)}{\omega_1(t)} \tag{7}$$

$$\mu_T(t) = \sum_{i=0}^{L-1} ip(i) \tag{8}$$

$$foTSU\ (th) = \phi_0 = max\left(\sigma_B^2(th)\right), 0 \leq th \leq L - 1 \tag{9}$$

$$0 < th < L - 1, i = 1, 2, 3 \dots k$$

When the histograms have a bimodal distribution and a deep and abrupt valley between the peaks, Otsu performs reasonably well. In the case of smaller object areas, the histogram may not possess bimodality. Also, if there is large additive noise, the histogram's sharp valley will get degraded. Then, there may be the segmentation error due to incorrect threshold values. As a result, tiny object size, a lower mean difference between background and foreground, significant variations between object and background pixels, a considerable quantity of noise, and other factors may limit object segmentation performance [73].

3.3. Kapur's method

Kapur's method can prove a valuable metric for multi-level segmentation [74]. Kapur [75] developed the Kapur's entropy technique in 1985, which maximized the histogram entropy of segmented classes to find the best threshold values. This method proves to be effective and feasible for image segmentation [76]. Shannon's entropy function is conceptualized as an inverse proportion between the probabilities of occurrence of an event and the information [77]. Higher the probability of occurrence of the event exhibits fewer information contents. The entropy presented by Shannon is given by the equation,

$$H = - \sum_{n=1}^{m} p_k \log(p_k) \tag{10}$$

where H- Entropy and Pk- the probability of the nth gray level, m-total number of levels in the gray image. The probability distribution considered here is between background and foreground in an image. The entropy of an image does not consider the spatial distribution of an image. Due to this, the same histogram having different images offers the same value of entropy and the threshold [77]. Assuming p1, p2, p3…p as the distribution of probability for a gray level image. Mostly, there are two probability

distributions to be considered. Eqs (11) and (12) define them as,

$$A: \frac{P_1}{P_s} \frac{P_2}{P_s} \dots \cdot \frac{P_s}{P_s} \tag{11}$$

$$B: \frac{P_{S+1}}{1-P_s} \frac{P_{S+2}}{1-P_s} \dots \cdot \frac{P_n}{1-P_s} \tag{12}$$

H(A) and H(B) gives the entropies associated with A and B in Eqs (13) and (14), respectively, The value of φs, which gives the sum of H(A) and H(B) has to be maximum, So that maximum information will be obtained between background and foreground.

$$H(A) = -\sum_{i=1}^{s} \frac{P_i}{P_s} \text{In} \frac{P_i}{P_s}$$

$$= -\frac{1}{P_s} \sum_{i=1}^{s} P_i In P_i - P_s In P_s \tag{13}$$

$$= In P_s + \frac{H_s}{P_s}$$

$$H(B) = -\sum_{1+s}^{n} \frac{P_i}{1-P_s} In \frac{P_i}{1-P_s}$$

$$= -\frac{1}{1-P_s} [\sum_{i=1+s}^{n} P_i \, In \, P_i - 1 - P_s \, In(1-P_s)] \tag{14}$$

$$= In(1-P_s) \frac{H_n - H_s}{1-P_s}$$

$$\phi_s = H_A + H_B = In P_s + \frac{H_s}{P_s} + In(1-P_s) + \frac{H_n - H_s}{1-P_s} \tag{15}$$

$$\phi_s = In \, P_s(1-P_s) + \frac{(H_n - H_s)P_s + H_s(1-P_s)}{P_s(1-P_s)} \tag{16}$$

The threshold value is obtained from Eq (16) of φs where it is maximum, after considering the discrete values of s in the equation. To get the exact distinction between backgrounds and foreground, the maximum value of φs is considered. Most techniques consisting of the metaheuristic approach for optimization follow a similar technique [78], where the fitness function is the entropy to maximize output. Multilevel thresholding using the Kapur approach is always superior to the single level to get more precise and accurate results, as the image segmentation is considered, as follows by Eq (16) [79]. This entropy-based method considers the histogram of a gray level as the base. There will be scattered in the optimal threshold as the entropy reaches maximization:

$$H(0) = -\sum_{i=0}^{t_1-1} \frac{P_i}{P_0} In \frac{P_i}{P_0}, P_0 = \sum_{i=0}^{t-1} P_i \tag{17}$$

$$H(1) = -\sum_{i=0}^{t_2-1} \frac{P_i}{P_1} In \frac{P_i}{P_1}, P_1 = \sum_{i=0}^{t_2-1} P_i \tag{18}$$

$$H(2) = -\sum_{i=0}^{t_3-1} \frac{P_i}{P_2} In \frac{P_i}{P_2}, P_2 = \sum_{i=0}^{t_3-1} P_i \tag{19}$$

$$H(j) = -\sum_{i=t_j}^{t_{j+1}-1} \frac{P_i}{P_j} In \frac{P_i}{P_j}, P_j = \sum_{i=t_j}^{t_{j+1}-1} P_i \tag{20}$$

$$H(m) = -\sum_{i=t_m}^{L-1} \frac{P_i}{P_m} In \frac{P_i}{P_m}, P_m = \sum_{i=t_m}^{L-1} P_m \tag{21}$$

The objective function is to maximize when selecting the optimal threshold.

$$f_{\text{kapur}}(th) = \phi_k = \text{argmax} - \sum_{i=1}^{m} H_i(th), 0 \leq th \leq L - 1 \tag{22}$$

Optimal threshold values for multiple thresholds are given as:

$$f_{\text{kapur}}(TH) = f_{\text{kapur}}(th_i), i = 1,2,3 \ldots., k \tag{23}$$

$th1, th2, \ldots$are the threshold values combined in a vector TH, I represent a specific class as provided in Eq (2).

3.4. TLBO optimization

Researchers have developed a variety of optimization algorithms [80]. There are certain popular categories of these algorithms. As the image segmentation is considered, some optimization algorithms such as genetic algorithm (GA) [81], particle swarm optimization (PSO) [82], ant bee colony (ABC) [83], etc. are presented. A newly developed algorithm by [61] is based on the classroom's teaching-learning process, TLBO. Some popular variants of these algorithms include basic, modified [84], differential learning approach [85], nonlinear inertia weighted approach [86], approach with learning experience from others [87], generalized oppositional approach [88], etc. In addition to these variants of TLBO, there is a recently developed variant known as LEBTLBO. Singh et al. [26] compared this optimization technique with GA, PSO and other popular traditional techniques for segmentation. They found that LebTLBO explores the segmentation with greater significance. For the segmentation problem of leukemia detection, the same optimization algorithm is adopted along with multi-level thresholding as an objective function here. This involved the classroom behavior of the teaching and learning process. Therefore, it has two phases- the teaching phase and the learning phase. Simple implementation and fast convergence are the main advantages of this algorithm. This basic algorithm is applied to many problems related to engineering, such as machining, drilling, ultrasonic machining, electrochemical machining, etc. [89], and also for image segmentation purposes [90]. There are certain modifications done are TLBO to enhance the search capability for finding the optimum solution. Although, as in traditional TLBO, every student is considered to have the same learning potential, LebTLBO works with the real-world problem related to enthusiasm for learning. More enthusiastic students in the class may also have good concentration and are keen to know the concepts taught to them by their teacher. On the contrary, less enthusiastic students may have less concentration towards teaching and are generally not open to getting information from teachers. LebTLBO is motivated by this kind of real-world teaching mechanism. In this approach, a third phase is introduced, called as "a poor phase of tutoring". Learning enthusiasm is calculated based on the grades of students. Students with good grades are considered to have higher learning enthusiasm and the students with less or lower grades are considered to have less learning enthusiasm.

3.4.1. Teacher phase of learning enthusiasm

Teaching learning is a unique process. The enthusiasm amongst the students towards learning defines the students as good students. This enthusiasm leads them to get good marks and also makes them interested to get the new knowledge from their teachers. When they gained knowledge from their

teacher, they will be able to pursue good marks in their examinations. After getting good grades, their positions will be altered and they will achieve good ranks, updating their positions to the top. On the other hand, the poor students or the students with less enthusiasm will surely get less marks and will not move towards the top positions. This behavior is the basis of teaching phase of the LebTLBO algorithm. Figure 5 shows different steps of the teacher phase. In the mathematical manner, it is explained as below.

For this phase to construct, there are two presumptions considered.

1) The students having decent evaluations are more excited about learning and are more open to getting information from the instructor.

2) The students with fewer evaluations have less energy for learning and are less open to acquiring knowledge from their instructor. In this phase, learners' grades are taken as the base for sorting them into the different categories from best to worst. For a maximization problem, an assumption is made that,

$$f(x_1) \geq f(x_2) \geq \cdots .. \geq f(X_K) \tag{24}$$

After this, learning enthusiasm values are defined as,

$$LE_i = LE_{min} + (LE_{max} - LE_{min})\frac{K-i}{K} \tag{25}$$

where, i=1, 2,. . . ., K, where LEmax and LEmin are the maximum and minimum value of enthusiasm of learners towards learning from their teacher. Depending upon the value of LE_i (learning enthusiasm value), students are classified into two categories as-gaining from the instructor or not gaining from the instructor. An irregular number is created for the student (xi) as ri ∈ [0, 1]. If ri ≤ LEi, the student will gain knowledge from his instructor. In the other case, the student will not be open to learning from the educator. When xi gains knowledge from his teacher, his position gets updated, and he gets upgraded his knowledge. Depending upon the learner's desire, whether to learn or not learn from the educator, the learner position will be updated with the following Eq (26).

$$x_{i,new}^d = f(x) = \begin{cases} x_{i,\text{old}}^d + rand_2 \cdot \left(x_{teacher}^d - T_F \cdot x_{mean}^d\right), & \text{if } rand_1 < 0.5 \\ \\ x_{r1}^d + F \cdot \left(x_{r2}^d + x_{r3}^d\right), & \text{otherwise} \end{cases} \tag{26}$$

where, r_1, r_2, r_3 are randomly selected integers from $\{1, 2, 3, \ldots NP\}$, $d \in \{1, 2, 3, \ldots D\}$, $rand_1$ and $rand_2$ are two random variables distributed uniformly between $[0,1]$, F is a scale factor in the range of $[0,1]$.
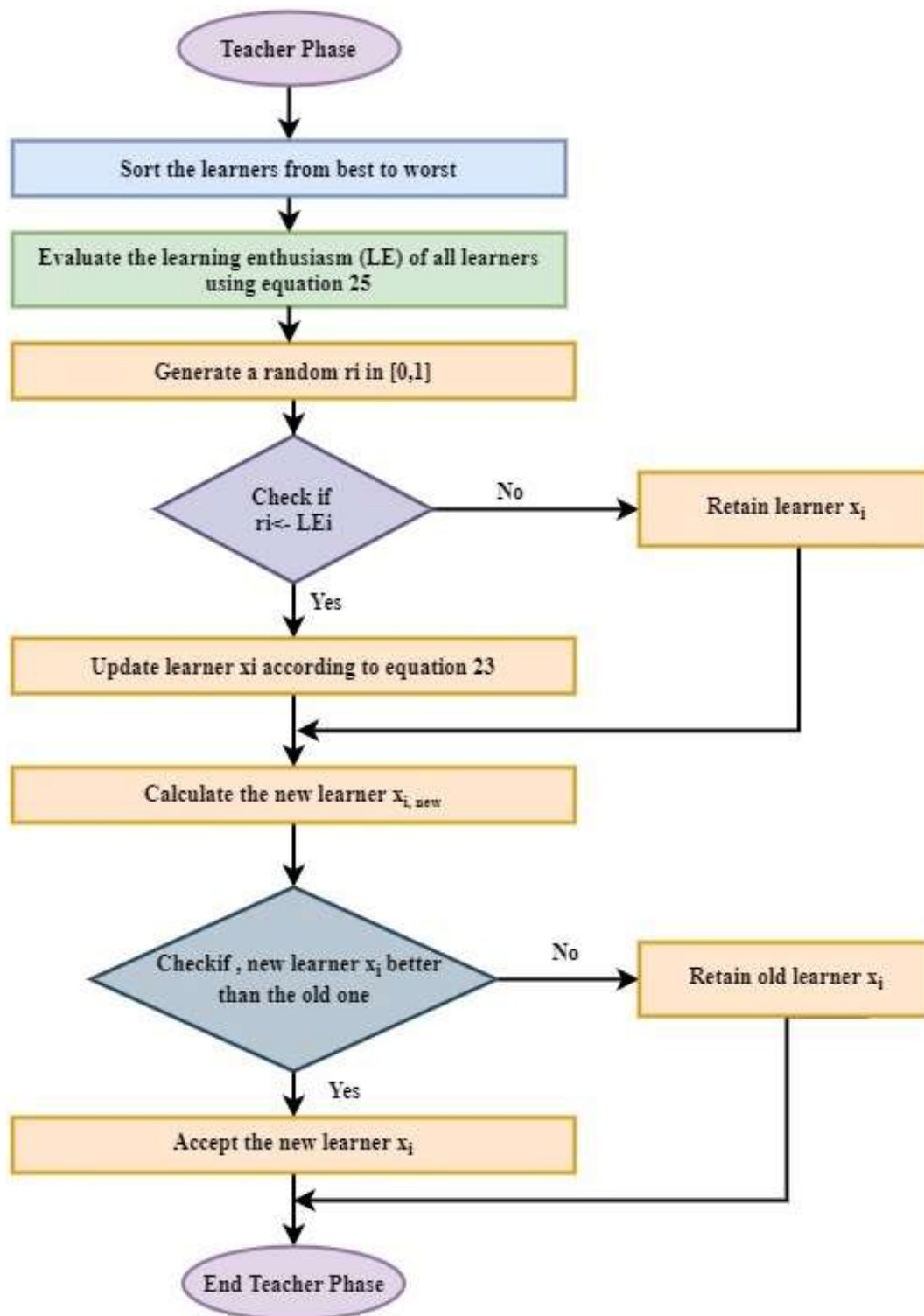
Figure 5. Teacher phase.

3.4.2.   Learning enthusiasm-based learner phase.

   The basis of this phase is the learners will learn from other learners depending on their desire towards learning. Their desire is lesser than the learning enthusiasm, then they will learn from other

learners. This means, the learners take the knowledge from other students also instead of the teacher. However, the position of the student is updated, only when it gains the knowledge from the teacher. Figure 6 shows different steps of the learner phase.
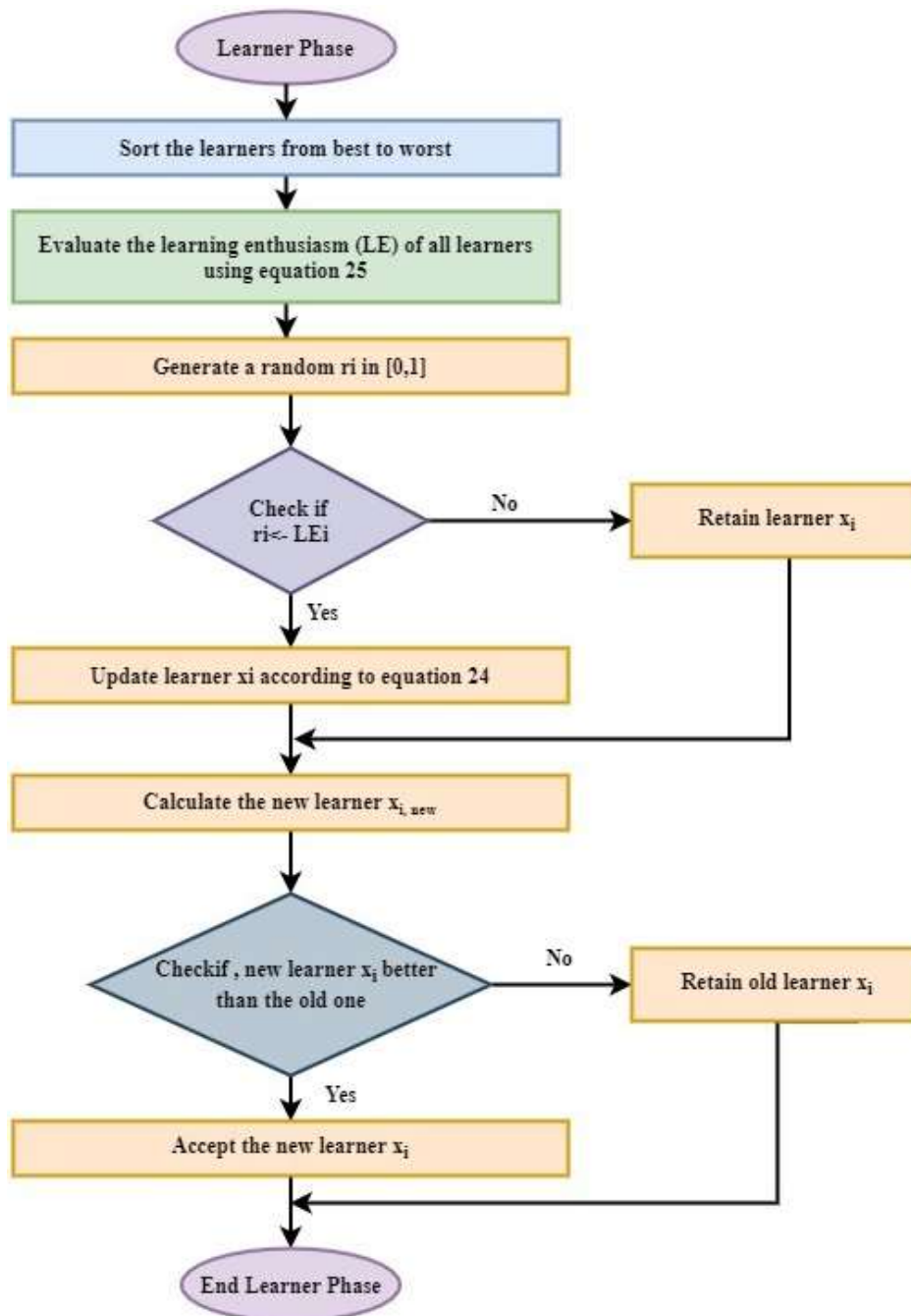

Figure 6. Learner phase.

The main assumption here is that learners with strong grades have a high level of learning excitement and that these learners have a high likelihood of gaining knowledge from their teachers. The students are rated from best to worst based on their grades for learning openness. This is based on Eq (25). A random number is created for the learner xi using the range of ri ∈ [0, 1]. If ri ≤ LEi, the

learner xi will learn from other learners; otherwise, the present learner xi will ignore the learner's knowledge of the learner. However, if current learner xi can obtain knowledge from the teacher, its position will be revised, taking into account diversity-enhanced teaching. This is shown in Eq (27),

$$x_{i,new}^d = \begin{cases} x_{i,old}^d + rand_2 \cdot (x_i - x_j) \; if \; f(x_i) \geq f(x_j) \\ x_{i,old}^d + rand_2 \cdot (x_j - x_i) \; if \; f(x_i) \leq f(x_j) \end{cases} \tag{27}$$

where, rand denotes a uniformly distributed random vector in the range [0,1], f(xi) denotes the objective function, and xi, old is the ith learner's old position. If xi, new is superior to xi, old, xi, new will be accepted. Otherwise, there will be no change in xi, old.

3.4.3. Poor student tutoring phase.

Poor students are sorted first and then amongst the poor students, the desire of gaining knowledge is again considered for categorizing them. The learning desire is considered for updating their grades in this case as well. This phase will work same as the learning phase, with a change that, the students considered here are below 10% level amongst all the students. This can be explained in the mathematical manner and is described in the following paragraph.

This phase differentiates the LebTLBO algorithm from the basic TLBO. Here, improvement in the grades of the poor students is the prime motive. The Poor learners are considered if they fall below the 10% level of the whole class. A learner named xT is picked randomly from among the impoverished student's xi, with a rank in the top half of the class.

The following Equation shows the learning,

$$x_{i,new}^d = x_{i,old}^d + rand(x_T^d - x_{i,old}^d) \tag{28}$$

where, d =1, 2, ...,D. In this phase also, xi, new will be accepted depending upon whether it is better than xi, old. Otherwise, it earlier remains unchanged. The flow chart of the same is shown in Figure 7. Those who receive good grades are more likely to alter their positions, whereas students who receive poor grades are less likely to do so. This strategy is based on the real-time teaching-learning process. Therefore, it proves more feasible in its working regarding the position updating of learners.

3.4.4. Optimizing Otsu and Kapur with LEbTLBO.

In this approach, Otsu and Kapur methods are given by Eqs (9) and (22), fkapur (TH) and fOTSU (TH) are considered as the objective functions for the optimization. Multiple optimal threshold values are to be found with the maximization of the objective function. Let thi = (thi1, thi2, ..., thik) denotes the population vector of ith position of different threshold values-k, where thi(j) ∈ 0, 255. Equation (29) gives the initial population of students,

$$th_i(j) = th_{min} + rand() \quad * (th_{max} - th_{min}) \tag{29}$$

where th_{min} and th_{max} are the image's minimum and maximum intensity values, j is the number of threshold levels, and a rand is a random number, respectively. Otsu and Kapur's entropy is used to calculate each's fitness value. The student with the maximum knowledge gives the best objective function for the algorithms.
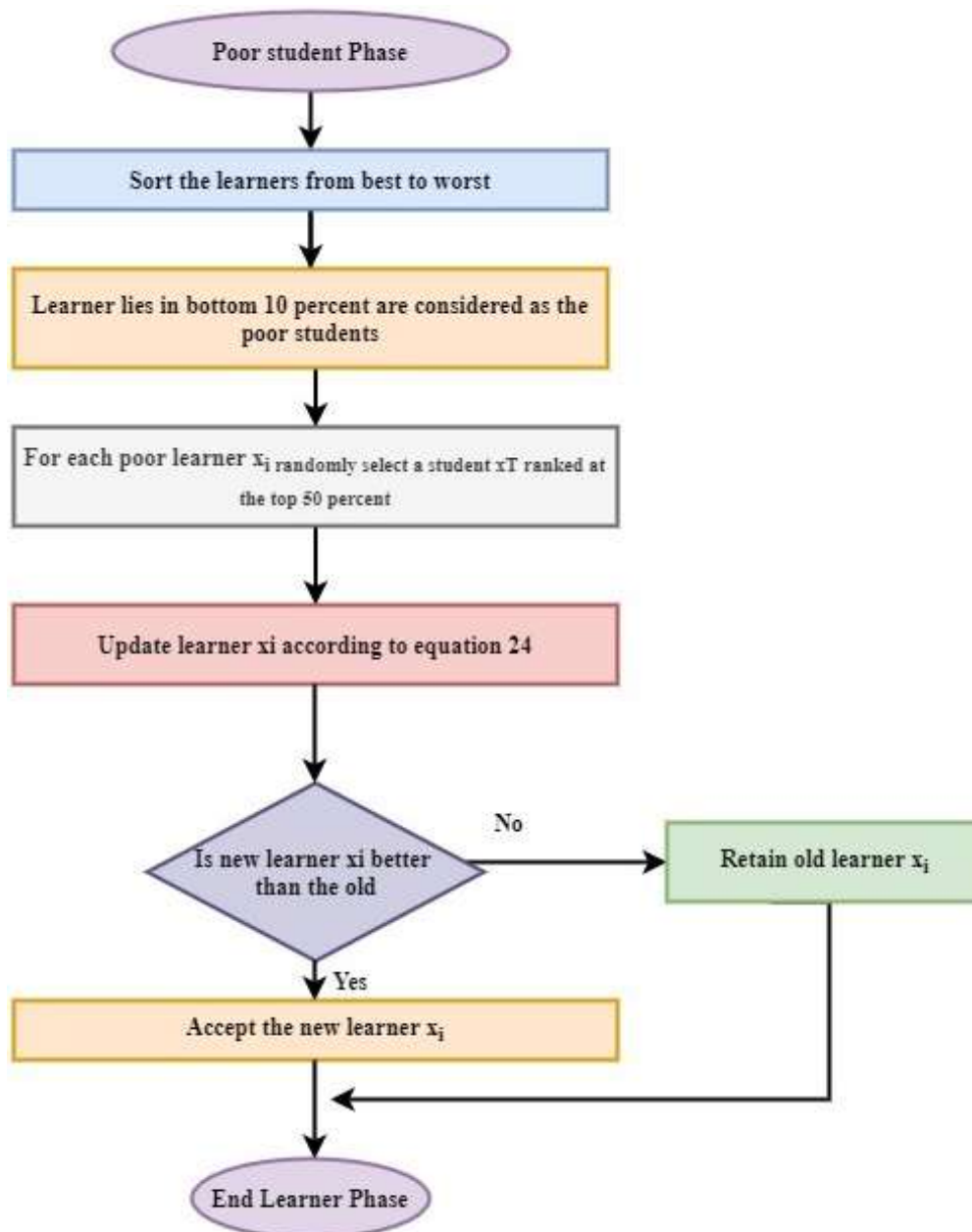
Figure 7. Poor phase.

For segmentation, the personal laptop is used with 8 GB of RAM and Intel-core I-5 processor. In addition, the Python software with version 3.8 is utilized for the same.

4. Performance evaluation metrics

Segmentation is the method for extraction of the region of interest for the given application. The first thing to evaluate segmentation performance is to compare the segmented image with the ground truth image. In this respect, different measures are identified for the evaluation of the system's performance. These parameters include volume overlapping error [91], dice index [92], relative volume difference [92], jaccard index [93], mean-square-error and peak-signal-to-noise-ratio [94].

4.1. Volume overlapping error (VOE)

For this to evaluate, segmented images and the ground truth masks are considered in their volumes. It is given by,

$$VOE = \frac{A \text{ and } B}{A \text{ or } B} \tag{30}$$

where, A= ground truth image, B= segmented image

The volumes of both images are compared and considered to be overlapped on each other. The amount of overlap indicates the correct segmentation. The amount of volume which does not overlap indicates the error in segmentation. The amount of non-overlapping between two images gives the overlapping error. Its value should be lesser to indicate effective segmentation.

4.2. Relative volume difference (RVD)

It evaluates the difference between the segmented image and the mask image which is the ground truth. It is given by,

$$RVD = \frac{A-B}{B} \tag{31}$$

where, A = ground truth image, B = segmented image.

In this performance metric, the ground truth image is subtracted from the segmented image. So its value will be lesser when the segmentation is effective. Less or zero value of this parameter indicates that, the segmented image and the mask image are exactly similar, showing the correct segmentation.

4.3. Jaccard index

This accuracy metric will compare the ground truth mask (a mask prepared manually by a medical professional, such as a radiologist or a pathologist) against the mask developed using segmentation.

$$JaccardIndex = \frac{A \text{ and } B}{A \text{ or } B} = \frac{TP}{TP+FN+FP} \tag{32}$$

where, TP = true positive, FN = false negative, FP = false positive.

It is also given in terms of dice score as,

$$JaccardIndex = \frac{Dice\ Score}{2-Dic\ Score} \tag{33}$$

4.4. Dice coefficient

Jaccard index and the dice coefficient are quite similar. The intersection is counted twice with the dice coefficient (TP). It is given by,

$$Dice\ score = \frac{2 \times (A \text{ and } B)}{(A \text{ and } B) + (A \text{ or } B)} \tag{34}$$

Jaccard index and dice coefficients indicates the number of truly segmented images out of the

total images. As the expectation of effective segmentation is that, all the images are to be segmented. Hence, the value of Jaccard index and dice coefficient should be as large as possible. Its maximum value is 1 [95].

4.5. Mean square error (MSE)

It calculates the squared error between the estimator and the estimated average. This parameter can analyze the segmentation performance.

4.6. Peak signal-to-noise ratio (PSNR)

It is the ratio of the signal with noise that signifies the loss during the segmentation process. It is expressed in dB with the following equation,

$$PSNR = 10 \, log_{10} \frac{peakvalue^2}{MSE} \tag{35}$$

MSE and PSNR are both used for getting the segmentation performance. MSE gives the error between mask image and the segmented image, while PSNR gives the signal-to-noise ratio. MSE value should be as low as possible to effective segmentation. MSE should always be lesser to indicate error-free segmentation. According to Eq (35), with lesser value of MSE, PSNR will lead to a greater value. According to the theory, the higher the PSNR, the better the degraded image has been reconstructed to match the original image, and the reconstructive algorithm is better.

4.7 Intersection over union (IoU)

Intersection over union (IoU) [96] is a type of image segmentation evaluation matrix that measures how much the goal ground truth mask overlaps with the prediction output. It is calculated by dividing the intersection of target and prediction pixels by the total number of pixels in both masks. According to Eq (36), IoU value will approach to high for error-free segmentation.

$$IoU = \frac{Target \cap Prediction}{Target \cup Prediction} \tag{36}$$

4.8 Structural similarity index (SSIM)

The perceptual difference between two comparable images is measured using SSIM. The formula for calculating the similarity index (SI) is as follows [97]:

$$SI = \frac{m_{ab}2xy2m_am_b}{m_am_bx^2+y^2m_a^2+m_b^2} \tag{37}$$

where, x and y denote the mean values of images original image image1-K (i, j) and enhanced image image2-I (i, j) and ma2, mb2 and mab denotes the variance of image1-K (i, j), image2-I (i, j) and covariance of image1-K (i, j) and image2-I (i, j). This index is used to get the structural similarity between the ground truth image and the segmented image. Hence, its value should be higher to indicate good segmentation. Its maximum value will be 1.

4.9. Mean absolute error (MAE)

It is defined as the difference between the original and improved image [98] and is expressed as below,

$$MAE = \frac{1}{n}\sum_{i=0}^{n} |f_i - y_i| = \frac{1}{n}\sum_{i=1}^{n} |e_i| \tag{38}$$

where, f_i is segmented images and y_i is the mask or ground truth image. This parameter finds the difference between the ground truth image and the segmented image. Hence, to show true segmentation, its value approach to zero.

5. Results

The results are visualized as shown in Figures 8–10. Figure 8a shows the original image of the dataset and the orange ring indicates the leukocyte to be segmented. Figure 8b is the mask, also called as ground truth image. It is obtained by manually segmenting the original image and the leukocyte is annotated by an expert pathologist. The segmentation task involves gray scaling of this original image, followed by the multi-level thresholding with Otsu and Kapur methods and then optimizing the performance with a popular LebTLBO optimization approach. Figures 9a,b are the segmented leukocytes by Kapur approach and optimized Kapur approach. In these Figures, the orange rings and the arrows indicate segmentation errors. Figure 10a,b are the outcomes of segmentation with Otsu and optimized Otsu approaches. These Figures indicate that optimized Otsu gives better segmentation as compared with other approaches in our proposed methodology.

In addition to the visualized results, different statistical parameters are also considered for the analysis of the performance of segmentation with our approach. Figure 11 shows the average results obtained as an outcome of segmentation on ALL-IDB dataset images.
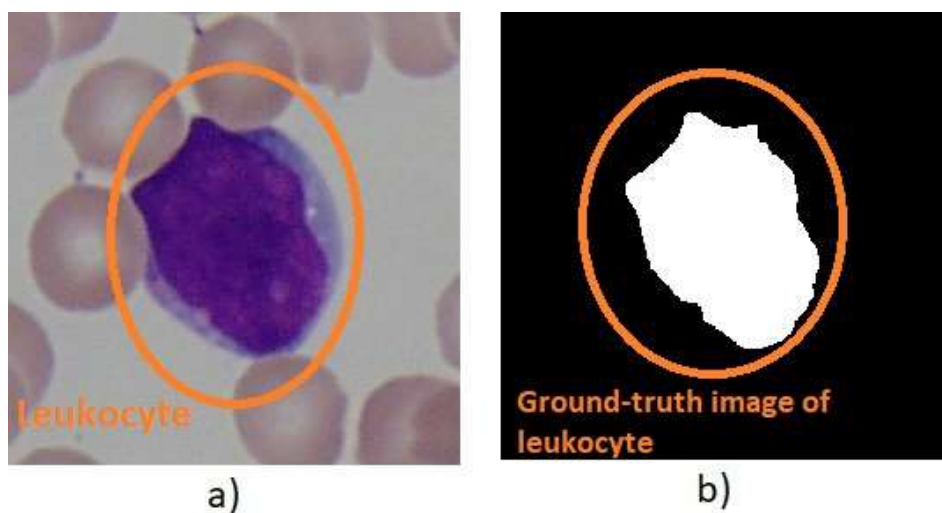

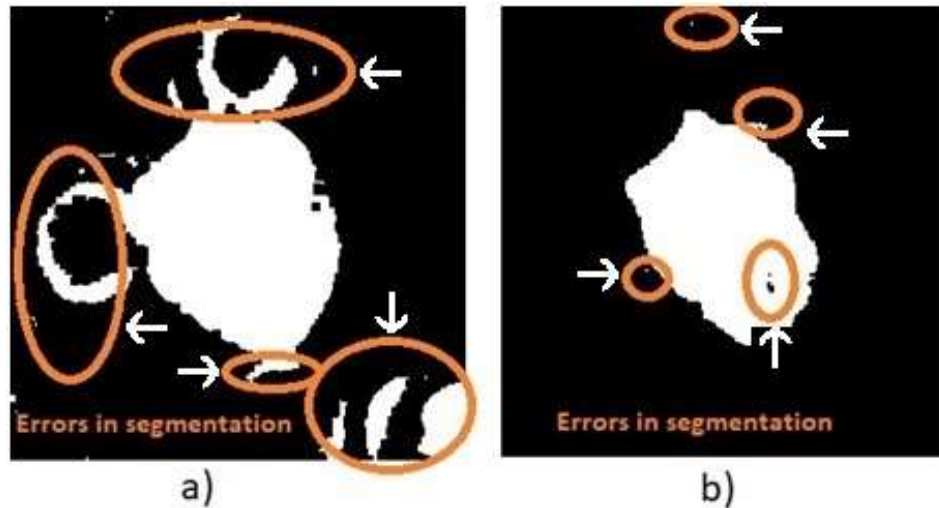**Figure 8.** a) Database image and b) Mask-Ground truth image.

Figure 9. a) Multi-Kapur segmented image. b) Multi-Kapur with LebTLBO segmentation.
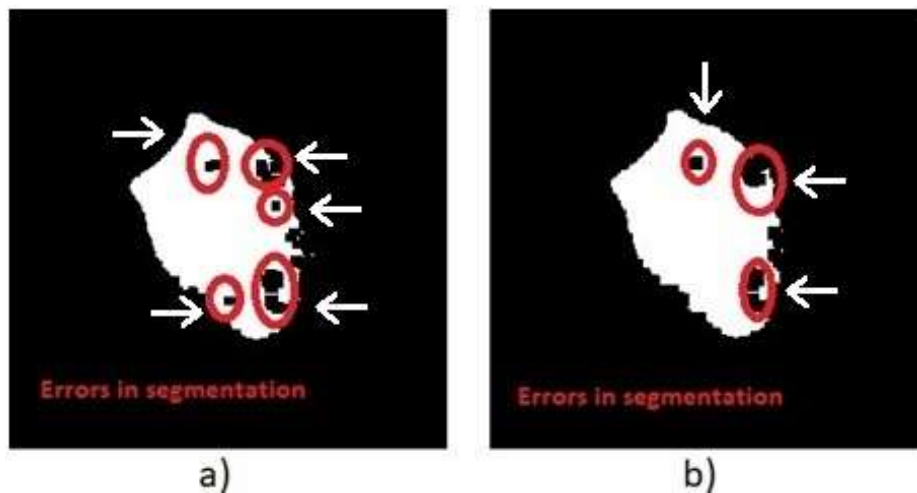

Figure 10. a) Multi-Otsu segmented image and b) Multi-Otsu with LebTLBO segmentation.

Jaccard index and dice coefficient are the indicators of the true positives with respect to the total images. These two parameters indicate the amount of segmentation. These parameter approach to the maximum value to show good segmentation. In our results, as indicated in Figure 11a),d) dice score and jaccard index are maximum when optimization is applied with basic Otsu and Kapur methods. This justifies the improvement in segmentation with optimized thresholding. Other parameter is VOE that gives the error in overlapping of volumes of ground truth image and the segmented image. This parameter is expected to have lower value ensuring the good segmentation. As shown in the Figure 11b), this error has less value in optimized Kapur approach. In addition to this, other popular error metrics are also evaluated for analyzing the segmentation performance. These include RVD, MSE, and MAE. As these are the errors in segmentation showing volume difference and mean errors, their value should also be lower to indicate good segmentation performance in our result visualization as shown in Figure 11c),e),i). These error parameters also show less values with optimized approach. Another parameter, SSIM is also evaluated as performance metric of segmentation. It shows similarities

between the ground truth image and the segmented image. The value of this parameter should be maximum to indicate good segmentation. As indicated in Figure 11h), SSIM has a maximum value with an optimized approach. The next metric for evaluation of segmentation performance is PSNR. Its value should be higher to ensure good segmentation. Also, in this case, optimized approach looks better than traditional thresholding approaches, as shown in Figure 11f). IoU is also considered as the performance metric, which gives higher value with optimized approach. This is indicated in Figure 11g).
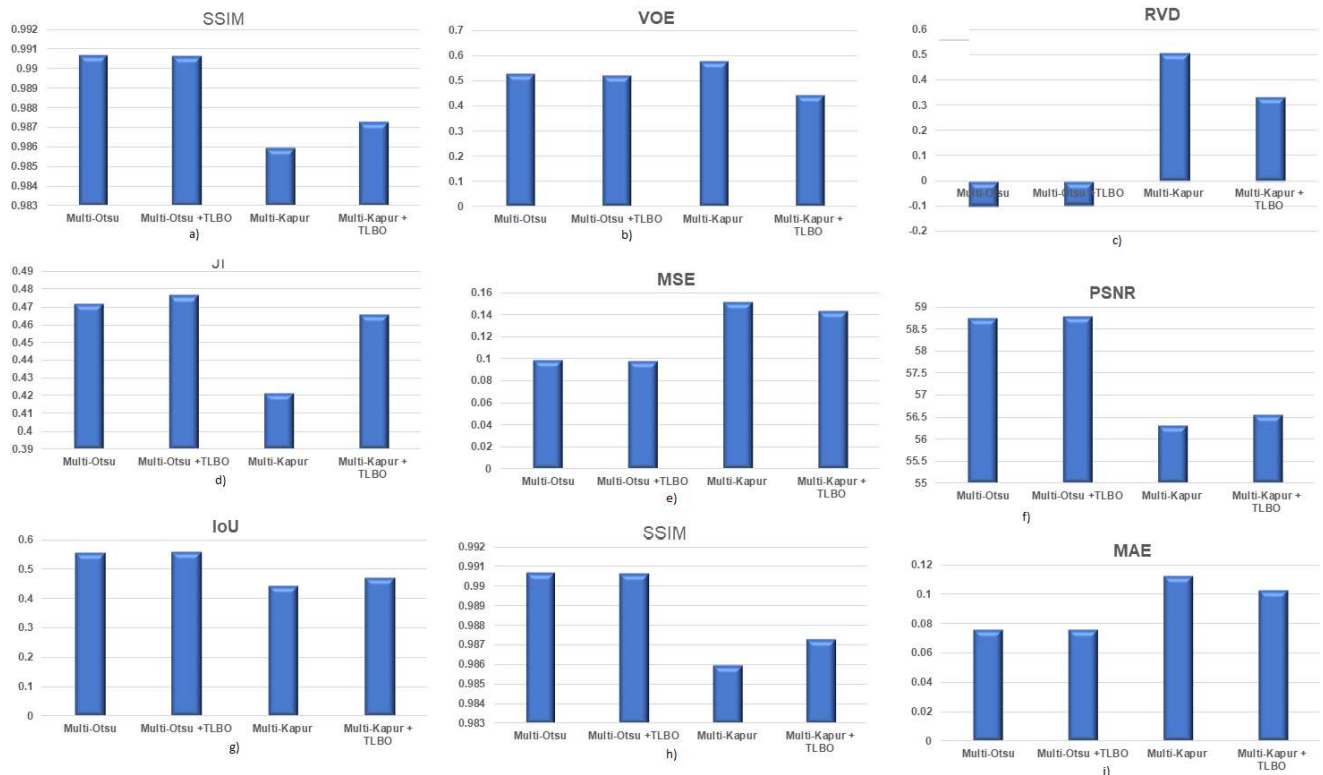
Figure 11. Variation of different scores with the proposed methods: a) dice score, b) VOE, c) RVD, d) JI, e) MSE, f) PSNR, g) IoU, h) SSIM and i) MAE.
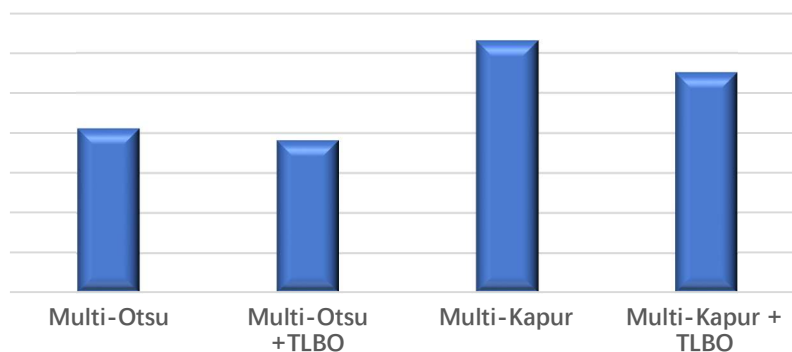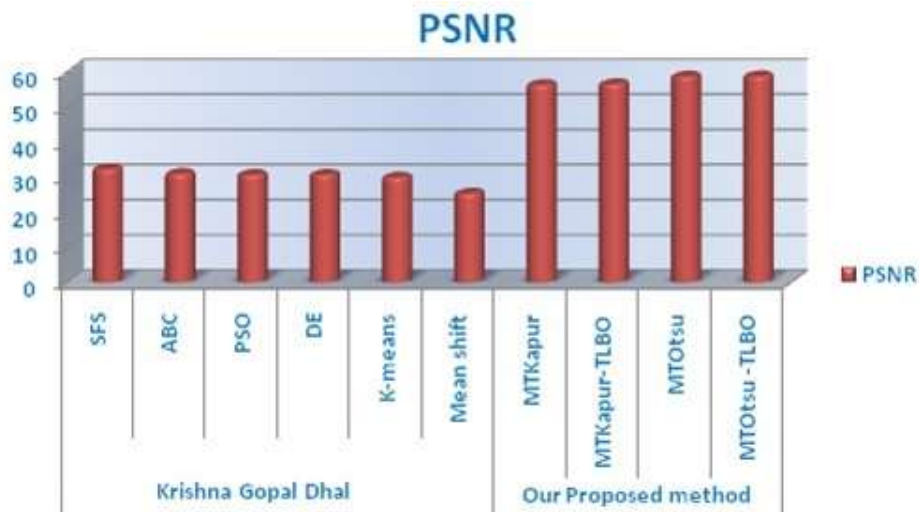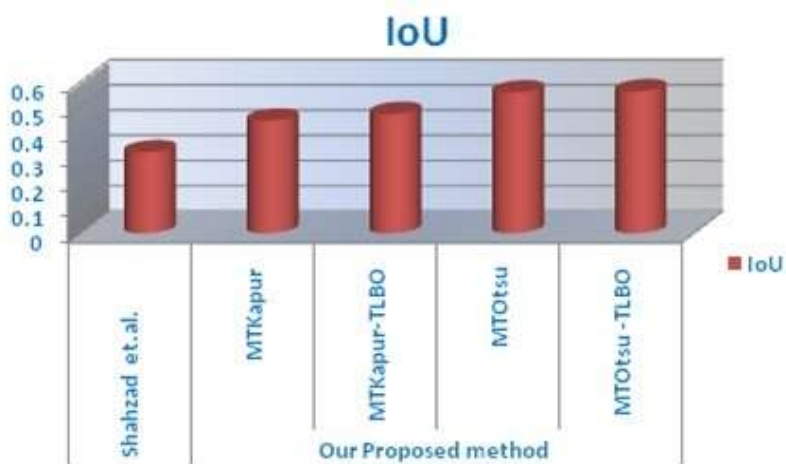
Figure 12. Execution time for segmentation with and without optimization.

a)

b)

c)

Figure 13. Comparison of the proposed method with others: in a) and b) comparison with et al. [99] with respect to PSNR and SSIM, respectively; in c) comparison with Shahzad et al [42].

In addition to these parameters, execution time analysis is performed. The time taken for segmentation for the traditional thresholding approach and with optimized approach is calculated. The time considered for single image segmentation with and without optimization. The visualization is shown in Figure 12. It indicates that optimized approaches require less time for segmentation.

The execution time analysis is also done with and without optimization which is shown in Figure 12. The segmentation is carried out on Core-I3 system with 4 GB RAM, and on Pycharm IDE platform. The segmentation time is considered for a single image with two thresholds.

The proposed approach is compared with the approach stated by Dhal et al. [99]. In their approach, the segmentation of leukocytes is presented by using some popular bio-inspired optimization algorithms and a clustering approach using K-means and mean shift. The bio-inspired optimization approaches used are stochastic fractal search (SFS), ant bee colony (ABC), particle swarm optimization (PSO) and differential evolution (DE). PSNR and similarity index are considered for comparison of these methods. This comparison is shown in Figure 13a)–c).

6. Discussion

Two thresholding methods, Otsu and Kapur, are used for segmentation. The search capabilities of these methods are improved by the LebTLBO optimization method. Otsu deals with the within-class and between-class variance, while Kapur has entropy as the thresholding parameter. Parameters considered for measuring the performance of the segmentation are Dice Score, which gives the relation of union and intersection between the segmented image and the ground truth image. As shown in Figure 11a, the dice score of the proposed methodology with Kapur and Optimized Kapur varies from 0.565731 to 0.60281, and the same for Otsu and Optimized Otsu varies from 0.628412 to 0.632528. This comparison indicates that Otsu thresholding with an optimization approach with LebTLBO gives a better dice score during segmentation evaluation. Jaccard index also varies from 0.466313 to 0.472316 for all four approaches. It also indicates the optimized Otsu offers good performance as the Jaccard index is considered.

The other parameter considered for evaluation is the relative volume difference, which is the difference in the volumes of mask-ground truth image and the segmented image. Its value is lesser in all four cases. Although, optimized Otsu indicates lesser RVD compared to the other three approaches with the value -0.0964. In addition to this, volume overlapping error is also considered for analysis. It gives AND and OR operations of ground truth image and segmented image. Its value lies between 0.44 to 0.52, while the lesser error is obtained in the optimized Kapur method. MSE and PSNR are other parameters considered for the evaluation of segmentation performance. MSE and MAE are also lesser in the Optimized Otsu approach with corresponding values of 0.0981 and 0.0761, respectively, indicating the lowest error with the optimized Otsu method. Regarding MSE, another parameter PSNR is considered, which should be larger for better segmentation. PSNR shows the signal-to-noise ratio, which also proves a parameter showing the segmented image quality compared to ground truth after segmentation. In the proposed methodology, it varies from 56.55 to 58.75, with different approaches. It also clearly states that Optimized Otsu proves to be better than other approaches.

IoU varies from 0.471 to 0.5573, indicating that, Optimized Otsu provides better IoU compared to other approaches in the methodology. The similarity index is also one more measure considered for analysis. Its value ranges from 0.9872 to 0.9906. Also, in this case, optimized Otsu proves to be a better segmentation approach.

Our proposed approach is found to offer a good comparative yield in terms of PSNR with the highest value of 58.80 with optimized Otsu, in comparison with approaches stated by [99]. In their methodology, PSNR varied from 25.43 to 32.39. The similarity index is another measure considered for comparison. It is found to be 0.99 in the case of our methodology, which is quite superior to the methodology proposed by [99], with a higher value of 0.8893 in the SFS approach.

Our methodology is also compared with the one proposed by Shahzad [42]. Here, the measure considered is IoU. Our approach gives IoU varying from 0.44 to 0.56, which is better than the measure obtained by [42] with a value of 0.3199.

Figures 9 and 10, shows the images as a result of segmentation with different methods. Kapur method shows an under segmentation (with more segmented regions than expected). When the optimization is applied, the segmentation is improved. Otsu has an over-segmentation (with fewer segmented regions than expected), and it is also improved with optimization. The main reason for the differential behavior of Otsu and Kapur is the basis of these two algorithms. Otsu works on maximization of between-class variance, whereas Kapur maximizes the entropy for measuring the homogeneity of the classes. Hence, the segmentation results differ with Otsu and Kapur. Although, optimization improves the segmentation results of both the algorithms.

In biological assays, there is a requirement of counting and segmentation of cells. This was considered to be a prospective research area of microscopic imaging. In practice, the manual counting of cell colony forming units is used to calculate the surviving fraction (SF) in clonogenic assays. This method is operator specific and may be prone to error. Furthermore, because of the fast development rate that causes nearby colonies to merge, determining the actual colony number is frequently impossible. The colony size, which is often connected with the given radiation dose or the administered cytotoxic agent, is not considered in traditional assessment. Researchers adopted different methodologies for these problems. These methods include Circular Hough Transform and adaptive thresholding [100], multi-level thresholding with feedback based on watershed algorithm [101], bilateral filtering followed by watershed transform and morphological filtering [102], binary classifier inspired by quantum machine learning theory with homogeneity considered to be the relevant feature [103]. The stated approach in our paper can be explored with the problem of clonological assay in biomedical field. Our proposed approach will provide novel insights related to the segmentation in biological assays.

7. Conclusions

In this research, an improved and optimized method for image segmentation is proposed and evaluated for the detection of leukemia via microscopic imaging. Images are taken from a popular and publicly available dataset ALL-IDB. Segmentation involved separation between background and foreground from microscopic images. Multi-level thresholding is applied for the segmentation purpose using two methods, Otsu and Kapur. Otsu is based on intensity, while Kapur is an entropy-based algorithm. The histogram is considered for the threshold selection in these cases. There is a problem of threshold selection with Otsu and Kapur if there are fewer histogram changes that lead to improper threshold values. So the performance of the system is boosted by optimizing the same with the LebTLBO optimization algorithm. This has increased the search capacity of the algorithm for getting proper threshold values for segmentation. Different parameters used for the analysis of segmentation, performance indicates the assurance of the optimization technique to improve the segmentation

performance. A comparative analysis of the proposed approach is done against the segmentation with bio-inspired optimization techniques such as SFS, ABC, PSO and clustering algorithm such as K-means and, other algorithms including DE and mean shift for segmentation purpose of leukocyte with the same dataset ALL-IDB. Performance measures such as PSNR and Similarity index are considered and the proposed approach was found to be better in terms of both parameters. The comparison is performed with a convolutional encoder- decoder framework with VGG-16 model, where IoU is the measure considered for the comparison. This system proved to be better over bio-inspired and some clustering algorithms. Therefore, for leukocyte detection, LebTLBO optimization will prove better than bio-inspired and clustering systems. These segmented images could be used further for the classification and diagnosis of leukemia. This work comes under traditional image processing, hence is always self-explainable and could always be more trusted than the unexplainable natures of newly developed AI techniques.

In the proposed methodology, an ALL-IDB database is utilized. This methodology is to be tested with other available databases of leukemia and with real patients' microscopic images, in order to prove the robustness of the proposed algorithm. Generative Adversarial Networks (GAN) could be employed further for improvement in segmentation performance. GAN could be combined with a transfer learning approach (TLA) for further enhancement in system performance.

Acknowledgement

Conflict of interest

The authors declare not competing interests.

References

1. N. M. Deshpande, S. S. Gite, R. Aluvalu, A brief bibliometric survey of leukemia detection by machine learning and deep learning approaches, *Lib. Philo. Pract.*, **4569** (2020).
2. S. Shafique, S. Tehsin, S. Anas, F. Masud, Computer-assisted acute lymphoblastic leukemia detection and diagnosis, in *2nd International Conference on Communication, Computing and Digital Systems*, (2019), 184–189.
3. H. Singh, G. Kaur, Automatic detection of blood cancer in microscopic images: a review, *Int. J. Innovations. Adv. Comput. Sci.*, **6** (2017), 40–43.
4. G. Biji, S. Hariharan, White blood cell segmentation techniques in microscopic images for leukemia detection, *IOSR J. Dental Med. Sci.*, **15** (2016), 45–51.
5. E. U. Alam, S. Banik, L. Chowdhury. A statistical approach to classify the leukemia patients from generic gene features, in *2020 International Conference on Computer Communication and Informatics*, (2020), 1–6.

6. H. M. Amin, Y. Yang, Y. Shen, E. H. Estey, F. J. Giles, S. A. Pierce, et al., Having a higher blast percentage in circulation than bone marrow: clinical implications in myelodysplastic syndrome and acute lymphoid and myeloid leukemias., *Leukemia*, **19** (2005), 1567–1572. doi: 10.1038/sj.leu.2403876.

7. C. Matek, S. Schwarz, K. Spiekermann, C. Marr, Human-level recognition of blast cells in acute myeloid leukaemia with convolutional neural networks, *Nat. Mach. Intell.*, **1** (2019), 538–544. doi: 10.1038/s42256-019-0101-9.

8. N. M. Deshpande, S. S. Gite, R. Aluvalu, Microscopic analysis of blood cells for disease detection: a review, *Tracking. Pre. Dis. Artif. Intell.*, **206** (2022), 125–151. doi: 10.1007/978-3-030-76732-7-6.

9. *Leukemic-versus-normal-blood*, 2021. Available from: https://www.shutterstock.com/image-illustration/leukemic-versus-normal-blood-73621156.

10. F. Al-Tahhan, A. A. Sakr, D. A. Aladle, M. Fares, Improved image segmentation algorithms for detecting types of acute lymphatic leukemia, *IET Image Process.*, **13** (2019), 2595–2603.

11. S. Mohapatra, D. Patra, S. Satpathi, Image analysis of blood microscopic images for acute leukemia detection, in *2010 International Conference on Industrial Electronics, Control and Robotics IEEE*, (2010), 215–219.

12. N. M. Deshpande, S. S. Gite, A brief bibliometric survey of explainable ai in medical field, *Lib. Philo. Pract.*, (2021), 1–27.

13. A. Khashman, E. Al-Zgoul, Image segmentation of blood cells in leukemia patients, *Rec. Adv. Comput. Eng. Appl.*, **2** (2010), 104−109.

14. B. Houwen, Blood film preparation and staining procedures, *Clin. Lab. Med.*, **22** (2002), 1–14.

15. B. Nwogoh, A. Adewoyin, Peripheral blood film: a review, *Ann. Ib. Postgrad. Med.*, **12** (2014), 71–79.

16. N. M. Deshpande, S. S. Gite, R. Aluvalu, A review of microscopic analysis of blood cells for disease detection with ai perspective, *PeerJ Comput. Sci.*, **7** (2021), **e460**. doi: 10.7717/peerj-cs.460.

17. M. Makem, A. Tiedeu, An efficient algorithm for detection of white blood cell nuclei using adaptive three stage PCA-based fusion, *Inform. Med. Unlocked*, **20** (2020), 100416. doi: 10.1016/j.imu.2020.100416.

18. P. Guruprasad, Overview of different thresholding methods in image processing, in *TEQIP Sponsored 3rd National Conference on ETACC*, (2020).

19. S. K. Dubey, S. Vijay, A review of image segmentation using clustering methods, *Int. J. Appl. Eng. Res.*, **13** (2018), 2484−2489.

20. H. G. Kaganami, Z. Beiji, Region-based segmentation versus edge detection, in *Fifth International Conference on Intelligent Information Hiding and Multimedia Signal Processing*, (2009), 1217−1221. doi: 10.1109/IIH-MSP.2009.13.

21. M. Mueller, K. Segl, H. Kaufmann, Edge-and region-based segmentation technique for the extraction of large, man-made objects in high-resolution satellite imagery, *Pattern Recognit.*, **37** (2004), 1619−1628. doi: 10.1016/j.patcog.2004.03.001.

22. C. Amza, *A review on neural network-based image segmentation techniques*, 2012. Available from: https://www.researchgate.net/profile/Catalin-Gheorghe-Amza-2/publication/228873725.

23. J. Rogowska, Overview and fundamentals of medical image segmentation, *Academic Press*, (2009), 73–90.

24. A. Singh, S. Sawan, M. Hanmandlu, V. K. Madasu, B.C. Lovell, An abandoned object detection system based on dual background segmentation, in *Sixth IEEE International Conference on Advanced Video and Signal Based Surveillance*, (2009), 352−357.

25. N. Mittal, A. Garg, P. Singh, S. Singh, H. Singh, Improvement in learning enthusiasm-based TLBO algorithm with enhanced exploration and exploitation properties, *Nat. Comput.*, **20** (2021), 577–609. doi: 10.1007/s11047-020-09811-5.

26. S. Singh, N. Mittal, H. Singh, A multilevel thresholding algorithm using lebtlbo for image segmentation, *Neural. Comput Appl.*, **32** (2020), 16681–16706. doi: 10.1007/s00521-020-04989-2.

27. J. S. Chohan, N. Mittal, R. Kumar, Parametric optimization of fused deposition modeling using learning enthusiasm enabled teaching learning based algorithm, *SN Appl. Sci.*, **2** (2020), 1–2. doi: 10.1007/s42452-020-03818-4.

28. X. Chen, B. Xu, K. Yu, W. Du, Teaching learning-based optimization with learning enthusiasm mechanism and its application in chemical engineering, *J. Appl. Math.*, **2018** (2018), 1806947. doi: 10.1155/2018/1806947.

29. M. Yildirim, A. C. Cinar, Classification of white blood cells by deep learning methods for diagnosing disease, *Rev. Artif. Intell.*, **33** (2019), 335–340. doi: 10.18280/ria.330502.

30. J. N. Kapur, P. K. Sahoo, A. K. Wong, A new method for gray level picture thresholding using the entropy of the histogram, *Comput. Vis. Graphics. Image Process.*, **29** (1985), 273–285. doi: 10.1016/0734-189X(85)90125-2.

31. A. S. Negm, O. A. Hassan, A. H. Kandil, A decision support system for acute leukaemia classification based on digital microscopic images, *Alex. Eng. J.*, **57** (2018), 2319–2332. doi: 10.1016/j.aej.2017.08.025.

32. N. Pombo, P. Rebelo, P. Ara´ujo, J. Viana, Combining data imputation and statistics to design a clinical decision support system for postoperative pain monitoring, *Procedia Comput. Sci.*, **64** (2015), 1018–1025. doi: 10.1016/j.procs.2015.08.621

33. H. Miao, C. Xiao, Simultaneous segmentation of leukocyte and erythrocyte in microscopic images using a marker-controlled watershed algorithm, *Comput. Math. Methods Med.*, (2018), 1−10. doi: 10.1155/2018/7235795.

34. S. C. Neoh, W. Srisukkham, L. Zhang, S. Todryk, B. Greystoke, C. P. Lim, et al., An intelligent decision support system for leukaemia diagnosis using microscopic blood images, *Sci. Rep.*, **5** (2015), 1–14. doi: 10.1038/srep14938.

35. H. Miao, C. Xiao, Simultaneous segmentation of leukocyte and erythrocyte in microscopic images using a marker-controlled watershed algorithm, *Comput. Math. Methods Med.*, **1** (2018), 1–10. doi: 10.1155/2018/7235795.

36. P. P. Guan, H. Yan, Blood cell image segmentation based on the Hough transform and fuzzy curve tracing, *Int. Conf. Mach. Learn. Cybern.*, **4** (2011), 1696–1701. doi: 10.1109/ICMLC.2011.6016961.

37. S. Biswas, D. Ghoshal, Blood cell detection using thresholding estimation based watershed transformation with Sobel filter in frequency domain, *Procedia Comput. Sci.*, **89** (2016), 651–657. doi: 10.1016/j.procs.2016.06.029.

38. S. Mishra, B. Majhi, P. K. Sa, Texture feature based classification on microscopic blood smear for acute lymphoblastic leukemia detection, *Biomed. Signal. Process. Control.*, **47** (2019), 303–311. doi: 10.1016/j.bspc.2018.08.012.

39. Y. Duan, J. Wang, M. Hu, M. Zhou, Q. Li, L. Sun, et al., Leukocyte classification based on spatial and spectral features of microscopic hyperspectral images, *Opt. Laser. Technol.*, **112** (2019), 530–538. doi: 10.1016/j.optlastec.2018.11.057.

40. N. Salem, N. M. Sobhy, M. El Dosoky, A comparative study of white blood cells segmentation using otsu threshold and watershed transformation, *J. Biomed. Eng. Med. Imaging*, **3** (2016), 15. doi: 10.14738/jbemi.33.2078.

41. M. Poostchi, I. Ersoy, K. McMenamin, E. Gordon, N. Palaniappan, S. Pierce, et al., Malaria parasite detection and cell counting for human and mouse using thin blood smear microscopy, *J. Med. Imaging*, **5** (2018), 1−13. doi: 10.1117/1.JMI.5.4.044506.

42. M. Shahzad, A. I. Umar, M. A. Khan, S. H. Shirazi, Z. Khan, W. Yousaf, Robust method for semantic segmentation of whole-slide blood cell microscopic images, *Comput. Math. Methods Med.*, **2020** (2020). doi: 10.1155/2020/4015323.

43. T. G. Debelee, F. Schwenker, S. Rahimeto, D. Yohannes, Evaluation of modified adaptive k-means segmentation algorithm, *Com. Vis. Med.*, **5** (2019), 347–361. doi: 10.1007/s41095-019-0151-2.

44. M. Tuba, Multilevel image thresholding by nature inspired algorithms: A short review, *Comput. Sci. J. Mold.*, **66** (2014), 318–338.

45. A. S. Dar, D. Padha, Medical image segmentation: A review of recent techniques, advancements and a comprehensive comparison, *Int. J. Comput. Sci. Eng.*, (2019), 114−124. doi: 10.26438/ijcse/v7i7.114124.

46. F. Sadeghian, Z. Seman, A. R. Ramli, B. H. Kahar, M. I. Saripan, A framework for white blood cell segmentation in microscopic blood images using digital image processing, *Biol. Proced. Online*, (2009), 196−206. doi: 10.1007/s12575-009-9011-2.

47. J. Al-Muhairy, Y. Al-Assaf, Automatic white blood cell segmentation based on image processing, in *16th IFAC World Congress*, (2005), 1−6.

48. Y. Yang, Y. Cao, W. Shi, A method of leukocyte segmentation based on S component and B component images, *J. Innovative Opt. Health Sci.*, **7** (2014), 1−8. doi: 10.1142/S1793545814500072.

49. *The truth that stares us in the face in our blood panels,* 2021. Available from: http://extralymey.com/the-truth-that-stares-us-in-the-face-in-our-blood-panels.

50. N. Bakhashwain, A. Sagheer, Online tuning of hyperparameters in deep LSTM for time series applications, *Int. J. Intell. Eng. Syst.*, **14** (2021), 212–220. doi: 10.22266/ijies2021.0228.21.

51. *Common-hematology-tests*, 2021. Available from: https://askhematologist.com/common-hematology-tests/.

52. M. P. Starmans, S. R. van der Voort, J. M. C. Tovar, J. F. Veenland, S. Klein, W.J. Niessen, *Radiomics: Data mining using quantitative medical image features*, *Academic Press*, (2020), 429−456.

53. B. Panda, *A survey on application of population based algorithm on hyperparameter selection*, Department of Computer Science: Course 761: Semester 2, (2019), 1−9.

54. J. G. Barbedo, Impact of dataset size and variety on the effectiveness of deep learning and transfer learning for plant disease classification, *Comput. Electron. Agric.*, **153** (2018), 46–53. doi: 10.1016/j.compag.2018.08.013.

55. S. Christin, E. Hervet, N. Lecomte, Applications for deep learning in ecology, *Methods Ecol. Evol.*, **10** (2019), 1632–1644. doi: 10.1111/2041-210X.13256.

56. S.S. Khan, A. Ahmad, Cluster center initialization algorithm for K-means clustering, *Pattern. Recognit. Lett.*, **25** (2004), 1293–302. doi: 10.1016/j.patrec.2004.04.007.

57. E. Suganya, S. Sountharrajan, S. K. Shandilya, M. Karthiga, Iot in agriculture investigation on plant diseases and nutrient level using image analysis techniques, *In Internet of Things in Biomedical Engineering*, *Academic Press*, **2019** (2019), 117−130. doi: 10.1016/B978-0-12-817356-5.00007-3.

58. W. Wang, L. Duan, Y. Wang, Fast image segmentation using two-dimensional Otsu based on estimation of distribution algorithm, *J. Electr. Comput. Eng.*, **2017** (2017). doi: 10.1155/2017/1735176.

59. C. Huang, X. Li, Y. Wen, An otsu image segmentation based on fruitfly optimization algorithm, *Alexandria Comput. Vis. Graphics. Image Process.*, *Eng. J.*, **60** (2021), 183−188. doi: 10.1016/j.aej.2020.06.054.

60. R. Rao, Jaya: A simple and new optimization algorithm for solving constrained and unconstrained optimization problems, *Int. J. Ind. Eng. Comput.*, **7** (2016), 19–34. doi: 10.5267/j.ijiec.2015.8.004.

61. R. V. Rao, V. Patel, Multi-objective optimization of heat exchangers using a modified teaching-learning based optimization algorithm, *Appl. Math. Modell.*, **37** (2013), 1147–1162. doi: 10.1016/j.apm.2012.03.043.

62. R. Rao, V. Patel, An elitist teaching-learning-based optimization algorithm for solving complex constrained optimization problems, *Int. J. Ind. Eng. Comput.*, **3** (2012), 535–560. doi: 10.5267/j.ijiec.2012.03.007.

63. D. P. Kanungo, J. Nayak, B. Naik, H. S. Behera, Hybrid clustering using elitist teaching learning-based optimization: an improved hybrid approach of TLBO, *Int. J. Rough Sets Data Anal.*, **3** (2016), 1–9. doi: 10.4018/IJRSDA.2016010101.

64. R. D. Labati, V. Piuri, F. Scotti. All-idb: The acute lymphoblastic leukemia image database for image processing, in *2011 18th IEEE International Conference on Image Processing*, (2011), 2045–2048.

65. F. Scotti, Robust segmentation and measurements techniques of white cells in blood microscope images, in *2006 IEEE Instrumentation and Measurement Technology Conference Processsdings*, (2006), 43–48.

66. F. Scotti, Automatic morphological analysis for acute leukemia identification in peripheral blood microscope images, in *CIMSA. 2005 IEEE International Conference on Computational Intelligence for Measurement Systems and Applications*, (2005), 96–101.

67. K. G. Dhal, A. Das, S. Ray, J. G´alvez, S. Das, Nature-inspired optimization algorithms and their application in multi-thresholding image segmentation, *Arch. Comput. Methods Eng.*, **27** (2020), 855–888. doi: 10.1007/s11831-019-09334-y.

68. N. Senthilkumaran, S. Vaithegi, Image segmentation by using thresholding techniques for medical images, *Com. Sci. Eng: An Int. J.*, **6** (2016), 1−13.

69. S. Kotte, P. R. Kumar, S. K. Injeti, An efficient approach for optimal multilevel thresholding selection for gray scale images based on improved differential search algorithm, *Ain Sha. Eng. Jo.*, **9** (2018), 1043–1067. doi: 10.1016/j.asej.2016.06.007.

70. N. Otsu, A threshold selection method from gray-level histograms, *IEEE Trans. Syst., Man Cyber.*, **9** (1979), 62–66.

71. C. Wang, J. Yang, H. Lv, Otsu multi-threshold image segmentation algorithm based on improved particle swarm optimization, in *IEEE 2nd International Conference on Information Communication and Signal Processing*, (2019), 440–443.

72. P. Yang, W. Song, X. Zhao, R. Zheng, L. Qingge, An improved Otsu threshold segmentation algorithm, *Int. J. Comput Sci. Eng.*, **22** (2020), 146–153.

73. Y. Zhan, G. Zhang, An improved OTSU algorithm using histogram accumulation moment for ore segmentation, *Symmetry*, **11** (2019), 431. doi: 10.3390/sym11030431.

74. W. Ji, X. He, Kapur's entropy for multilevel thresholding image segmentation based on moth-flame optimization, *Math. Biosci. Eng.*, **18** (2021), 7110–7142. doi: 10.3934/mbe.2021353.

75. J. N. Kapur, P. K. Sahoo, A. K. Wong, A new method for gray-level picture thresholding using the entropy of the histogram, *Comput. Vis. Graphics. Image Process.*, **29** (1985), 273–285. doi: 10.1016/0734-189X(85)90125-2.

76. Z. Yan, J. Zhang, Z. Yang, J. Tang, Kapur's entropy for underwater multilevel thresholding image segmentation based on whale optimization algorithm, *IEEE Access*, **9** (2020), 41294–41319. doi: 10.1109/ACCESS.2020.3005452.

77. J. N. Kapur, P. K. Sahoo, A. K. Wong, A new method for graylevel picture thresholding using the entropy of the histogram, *Comput. Vis. Graphics. Image Process.*, **29** (1985), 273–285. doi: 10.1016/0734-189X(85)90125-2.

78. D. Feng, S. Wenkang, C. Liangzhou, D. Yong, Z. Zhenfu, Infrared image segmentation with 2-d maximum entropy method based on particle swarm optimization (pso), *Pattern. Recognit. Lett.*, **26** (2005), 597–603. doi: 10.1016/j.patrec.2004.11.002.

79. H. Liang, H. Jia, Z. Xing, J. Ma, X. Peng, Modified grasshopper algorithm-based multilevel thresholding for color image segmentation, *IEEE Access*, **7** (2019), 11258–11295. doi: 10.1109/ACCESS.2019.2891673.

80. M. Sánchez-Silva, C. Gómez, *Risk assessment and management of civil infrastructure networks: a systems approach*, Woodhead Publishing, (2013), 437−464.

81. C. Tan, Y. Sun, G. Li, B. Tao, S. Xu, F. Zeng, Image segmentation technology based on genetic algorithm, in *Proceedings of the 3rd International Conference on Digital Signal Processing*, (2019), 27−31. doi: 10.1145/3316551.3318229.

82. S. Ait-Aoudia, E. Guerrout, R. Mahiou, Medical image segmentation using particle swarm optimization, in *18th International Conference on Information Visualization*, (2014), 287−291, doi: 10.1109/IV.2014.68.

83. E. Cuevas, F. Sención-Echauri, D. Zaldivar, M. Pérez, *Image segmentation using artificial Bee colony optimization*, Springer, (2013), 965−990.

84. S. C. Satapathy, A. Naik, Modified teaching-learning-based optimization algorithm for global numerical optimization-a comparative study, *Swarm Evol. Comput.*, **16** (2014), 28–37. doi: 10.1016/j.swevo.2013.12.005.

85. F. Zou, L. Wang, D. Chen, X. Hei, An improved teaching learning-based optimization with differential learning and its application, *Math. Probl. Eng.*, **1** (2015), 1–20. doi: 10.1155/2015/754562.

86. Z. S. Wu, W. P. Fu, R. Xue, Nonlinear inertia weighted teaching learning-based optimization for solving global optimization problem, *Comput. Intell. Neursci.*, **1** (2015), 1–15. doi: 10.1155/2015/292576.

87. F. Zou, L. Wang, X. Hei, D. Chen, Teaching-learning-based optimization with learning experience of other learners and its application, *Appl. Soft Comput.*, **37** (2015), 725–736. doi: 10.1016/j.asoc.2015.08.047.

88. X. Chen, K. Yu, W. Du, W. Zhao, G. Liu, Parameters identification of solar cell models using generalized oppositional teaching learning based optimization, *Energy*, **99** (2016), 170–180. doi: 10.1016/j.energy.2016.01.052.

89. A. Tiwari, M. K. Pradhan, Applications of TLBO algorithm on various manufacturing processes: A review, *Mater. Today Proc.*, **4** (2017), 1644−1652. doi: 10.1016/j.matpr.2017.02.003.

90. B. S. Khehra, A. S. Pharwaha, Image segmentation using teaching-learning-based optimization algorithm and fuzzy entropy, in *15th International Conference on Computational Science and Its Applications*, (2015), 67−71. doi: 10.1109/ICCSA.2015.10.

91. V. Yeghiazaryan, I. Voiculescu, Family of boundary overlap metrics for the evaluation of medical image segmentation, *J. Med. Imaing*, **5** (2018), 015006. doi: 10.1117/1.JMI.5.1.015006.

92. S. Yousefi, N. Kehtarnavaz, A. Gholipour, Improved labeling of subcortical brain structures in atlas-based segmentation of magnetic resonance images, *IEEE Tran. Biomed. Eng.*, **59** (2011), 1808−1817. doi: 10.1109/TBME.2011.2122306.

93. J. Bertels, T. Eelbode, M. Berman, D. Vandermeulen, F. Maes, R. Bisschops, M. B. Blaschko, Optimizing the dice score and jaccard index for medical image segmentation: Theory and practice, in *International Conference on Medical Image Computing and Computer-Assisted Intervention*, (2019), 92−100. doi: 10.1007/978-3-030-32245-8_11.

94. S. J. Jemila, A. B. Therese, Selection of suitable segmentation technique based on image quality metrics, *Imaing Sci. J.*, **67** (2019), 475−480. doi: 10.1080/13682199.2020.1718298.

95. A. Oulefki, S. Agaian, T. Trongtirakul, A. K. Laouar, Automatic COVID-19 lung infected region segmentation and measurement using CT-scans images, *Pattern Recognit.*, **114** (2021). doi: 10.1016/j.patcog.2020.107747.

96. A. Rahman, Y. Wang, Optimizing intersection-over union in deep neural networks for image segmentation, in *Proceedings of the International Symposium on Visual Computing*, (2016), 234−244.

97. Z. Wang, A. C. Bovik, H. R. Sheikh, E. P. Simoncelli, Image quality assessment: from error visibility to structural similarity, *IEEE Trans. Image Process.*, **13** (2004), 600−612. doi: 10.1109/TIP.2003.819861.

98. D. Asamoah, E. Ofori, S. Opoku, J. Danso, Measuring the performance of image contrast enhancement technique, *Int. J. Comput. Appl.*, **181** (2018), 6−13.

99. K. G. Dhal, J. Gálvez, S. Ray, A. Das, S. Das, Acute lymphoblastic leukemia image segmentation driven by stochastic fractal search, *Multimed. Tools Appl.*, (2020), 1−29. doi: 10.1007/s11042-019-08417-z.

100. C. Militello, L. Rundo, V. Conti, L. Minafra, F. P. Cammarata, G. Mauri, et al., Area-based cell colony surviving fraction evaluation: A novel fully automatic approach using general-purpose acquisition hardware, *Comput. Biol. Med.*, **89** (2017), 454−465, doi: 10.1016/j.compbiomed.2017.08.005.

101. A. U. M. Khan, A. Torelli, I. Wolf, N. Gretz, AutoCellSeg: robust automatic colony forming unit (CFU)/cell analysis using adaptive image segmentation and easy-to-use post-editing techniques, *Sci. Rep.*, **8** (2018), 1−10. doi: 10.1038/s41598-018-24916-9.

102. L. Rundo, A. Tangherloni, D. R. Tyson, R. Betta, C. Militello, S. Spolaor, et al., ACDC: Automated cell detection and counting for time-lapse fluorescence microscopy, *Appl. Sci.*, **10** (2020), 1−22. doi: 10.3390/app10186187.

103. G. Sergioli, C. Militello, L. Rundo, L. Minafra, F. Torrisi, G. Russo, et al., A quantum-inspired classifier for clonogenic assay evaluations, *Sci. Rep.*, **11** (2021), 1–10. doi: 10.1038/s41598-021-82085-8.